JGR Oceans

Key Points:
- It is demonstrated that channel deepening can explain the transition from low to high sediment concentrations in the Ems River Estuary
- A systematic analysis of the underlying physical processes shows that the transition is related to resonance of the M_4 tide
- Sediment-induced damping of turbulence is essential for reproducing the observed transition

Modeling the Transition to High Sediment Concentrations as a Response to Channel Deepening in the Ems River Estuary

Yoeri M. Dijkstra[1] , **Henk M. Schuttelaars**[1] , **George P. Schramkowski**[1,2], and **Ronald L. Brouwer**[1,2]

[1]Delft Institute of Applied Mathematics, Delft University of Technology, Delft, Netherlands, [2]Flanders Hydraulics Research, Antwerp, Belgium

Abstract Many estuaries are strongly modified by human interventions, including substantive channel deepening. In the Ems River Estuary (Germany and Netherlands), channel deepening between the 1960s and early 2000s coincided with an increase in the maximum near-bed suspended sediment concentration from moderate ($\sim$1 kg/m^3) to high (>10 kg/m^3). In this study the observed transition in the suspended sediment concentration in the Ems is qualitatively reproduced by using an idealized width-averaged iFlow model. The model is used to reproduce observations from 1965 and 2005 by only changing the channel depth between the years. Model results show an increase in sediment concentrations from approximately 1–2 kg/m^3 to 20–30 kg/m^3 near the bed between 1965 and 2005 if the river discharge is below 70 m^3/s, which holds approximately 60% of the time. Thereby, this study for the first time provides strong evidence for earlier published hypotheses that channel deepening was the main driver of the increased sediment concentrations in the Ems. The results are explained using two aspects: sediment transport (longitudinal processes) and local resuspension (vertical processes). The magnitude of the sediment import increased, because a combination of channel deepening and sediment-induced damping of turbulence increased the M_2–M_4 tidal asymmetry. This effect is particularly strong, because the M_4 tide evolved to a state close to resonance. All imported sediment is kept in suspension when it is assumed that resuspension is sufficiently efficient, which depends on the value of the erosion parameter used and inclusion of hindered settling in the model.

Plain Language Summary Between the 1960s and early 2000s, the sediment concentration observed in the Ems River Estuary (Germany and Netherlands) has increased strongly. This increased sediment concentration is relevant as it is associated with a severe deterioration of the ecosystem. During the same period, the estuary underwent multiple human interventions including substantive channel deepening to support large ships. This study demonstrates that the observed increase in sediment concentrations can be reproduced qualitatively using a computational model when only accounting for the change of depth between the 1960s and 2000s. Thereby, this study provides strong evidence for earlier published hypotheses that channel deepening is the main driver resulting in increased sediment concentrations. The used model is an idealized width-averaged model called iFlow. The model is idealized in the sense that it specializes in modeling the large-scale trends and uses simplified descriptions of some physical processes, focused on capturing the qualitative behavior. The model simplifications allow for a thorough and systematic analysis of the underlying physical processes and uncertainties. Using this analysis, a deeper understanding of the model results and related uncertainties is obtained.

1. Introduction

Estuaries are known to be efficient sediment traps, with sediment concentrated in one or more estuarine turbidity maxima (ETM). The maximum sediment concentrations in such ETM typically range between 0.1 and over 10 kg/m^3 and may be several times to orders of magnitude higher than in the surrounding waters. Several examples exist of estuaries that underwent a strong increase in the sediment concentration in their ETM, including the Ems (Germany and Netherlands) and Loire (France) Rivers (Winterwerp et al., 2013). Such a transition has severe consequences for the ecological functioning of the estuary, as high suspended sediment concentrations are associated with a strong reduction in oxygen levels (e.g., Talke, De Swart,
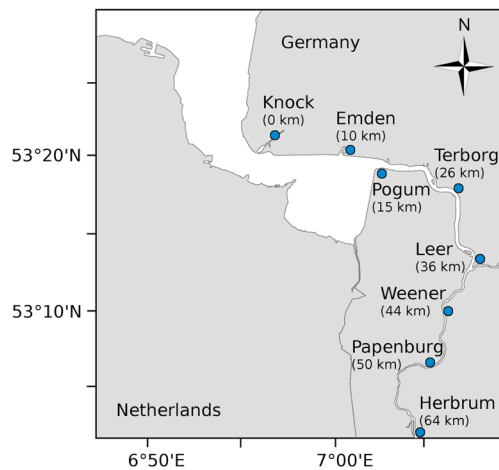
Figure 1. The Ems River Estuary, located in Northern Germany and Netherlands discharging into the Wadden Sea-North Sea. Our model domain is from Knock to the tidal weir at Herbrum, 64 km from Knock.

& De Jonge, 2009; Uncles et al., 1998) and primary production (Cloern, 1987). The increased sediment concentration in both the Ems and Loire Rivers is hypothesized to be due to man-made changes to the estuary in the last several decades, most notably deepening of the shipping channel (Winterwerp & Wang, 2013). Considering the large-scale deepening projects in many estuaries around the world, it is important to understand the effect of channel deepening on the sediment concentration in the Ems and Loire, to assess if a similar large increase in sediment concentration can happen in other estuaries as well.

In this study we focus on the Ems River Estuary; see Figure 1. In the 1950s, the ETM in the Ems River was located approximately between Pogum and Terborg (km 15–25), with typical concentrations at the surface estimated around 0.1–0.2 kg/m^3 (De Jonge et al., 2014) and at the bed around 0.5–2 kg/m^3 (Dechend, 1950). After dredging operations that occurred between 1960 and 1994, the ETM had moved upstream and had become a wide turbidity zone between approximately Pogum/Terborg (km 15–25) and the tidal weir at Hebrum (km 64). Typical sediment concentrations in this ETM are 1–4 kg/m^3 at the surface (De Jonge et al., 2014) and 10–100 kg/m^3 near the bed (Becker et al., 2018; Papenmeier et al., 2013; Talke, De Swart, & Schuttelaars, 2009; Wang, 2010).

Several modeling studies have focussed on this transition in the sediment concentration in the Ems. All studies to date have done so by calibrating their model separately for conditions before and after the transition. Using various models ranging from highly idealized to complex, it was found that a lower roughness is required to calibrate to conditions after the transition to high sediment concentrations (Chernetsky et al., 2010; Van Maren et al., 2015; Winterwerp et al., 2013). Using an idealized model and simultaneously deepening the channel and lowering the roughness, Chernetsky et al. (2010) and De Jonge et al. (2014) qualitatively reproduced the upstream shift in the ETM position. However, as their model assumed a prescribed amount of sediment in the estuary, they could not draw conclusions about the increase of the sediment concentration. Using a numerical three-dimensional model calibrated to recent conditions (year 2005), Weilbeer (2007) and Van Maren et al. (2015) obtained concentrations up to 10 kg/m^3 near the bed in the ETM, thereby demonstrating that it is possible to find high sediment concentrations in the model under suitable hydrodynamic conditions. However, in order to dynamically model the actual transition, the reduced roughness and increase in concentration should not follow from recalibration but have to be resolved by the model itself. It is thought that the reduced roughness is caused by damping of turbulence and bed friction by the high sediment concentrations (Winterwerp & Wang, 2013). Winterwerp and Wang (2013) and Van Maren et al. (2015) go one step further and hypothesize about the existence of a positive feedback loop, where a high sediment concentration leads to a reduction of the hydraulic roughness, which in turn leads to the import of more sediment. However, no study to date has shown that deepening of the estuary indeed leads to a highly increased import and trapping of sediment nor has it been shown that this imported sediment is indeed able to reduce the hydraulic roughness to the extent necessary to match observations.

The goal of this study is to show whether channel deepening alone can be responsible for the transition from low to high sediment concentrations in the Ems and what physical mechanisms underlie this transition. This is done by extending and using the idealized width-averaged process-based iFlow model (Dijkstra et al., 2017). Focus of the study is on the qualitative characteristics of the dynamic equilibrium state of the sediment concentration estuary for conditions of 1965 and 2005 (i.e., before and after the deepening operations) and the physical processes essential to establish this state. The model is calibrated only to conditions before deepening, and the model results after deepening are systematically analyzed for different parameters to verify the robustness of the results.

A short description of the iFlow model and the extensions is given in section 2. Section 3 presents the data used to set up the model. The results of the 1965 and 2005 cases for default parameter settings are presented in section 4 and further analyzed in section 5. The sensitivity of the results to several model parameters is discussed in section 6. Finally, the conclusions are summarized in section 7.

2. Model

The framework used for this study is an extended version of the *iFlow* model described by Dijkstra et al. (2017). iFlow is a width-averaged idealized model that solves for the continuity and momentum equations for the water motion and the mass balance equation for sediment. Several assumptions are made to speed up the model and allow for detailed analysis of the most important processes in the equations. First, it is assumed that the estuarine geometry can be parametrized by smoothed width and depth profiles, ignoring bathymetric variations on length scales much smaller than the length of the estuary. Second, it is assumed that the water surface elevation is small compared to the mean depth. This allows the use of scaling and perturbation methods, which leads to systems of mathematical equations that can be solved at low computational costs. Furthermore, it allows for making a decomposition of the water motion and sediment transport into contributions by individual physical forcing mechanisms. Third, the model resolves only the subtidal, M_2 and M_4 contributions to the water motion and sediment dynamics, imposing an M_2 tide and an M_4 tide at the mouth and a constant river discharge at the head of the estuary. The subtidal and tidal contributions are computed for a dynamic equilibrium. This means that the water motion and sediment concentration are allowed to vary on a tidal time scale but not on a subtidal time scale. Considering dynamic equilibrium prevents spin-up time, hence strongly reducing the computation time compared to models based on time stepping routines. Below, we discuss the elements of the model that are changed or added to the version presented in Dijkstra et al. (2017) in more detail.

The first change to the iFlow model is the parametrization of the erosion rate E, which here represents erosion of a soft nonconsolidated layer of fine sediments on top of a nonerodible layer. The erosion rate is written as the product of the potential erosion $\hat{E}$ and the erodibility f (Brouwer et al., 2018; Dijkstra et al., 2018), that is,

$$E = \hat{E} f. \tag{1}$$

The potential erosion $\hat{E}$ is the erosion rate assuming an abundant availability of sediment. The potential erosion is parametrized using the formulation of Partheniades (Kandiah, 1974) but assuming a negligible critical shear stress

$$\hat{E} = M|\tau_b|. \tag{2}$$

The parameter M is an erosion parameter, and τ_b represents the bed shear stress. The erodibility f takes values between 0 and 1 to account for the amount of sediment on the bed. If no easily erodible sediment is available at the bed at any time during the tidal cycle, $f = 0$ and consequently the erosion is zero. If easily erodible sediment is available at the bed during the entire tidal cycle, f equals one and $E = \hat{E}$. If easily erodible sediment is available at the bed only during a part of the tidal cycle, f takes a value between 0 and 1 (see Brouwer et al., 2018, for an elaborate discussion and derivation of the erodibility).

As a second extension to the model, the sediment settling velocity is allowed to vary along the channel due to the effects of hindered settling (Richardson & Zaki, 1954). Here we use a parametrization of hindered settling in which the settling velocity in each water column is based on the subtidal near-bed sediment concentration, according to

$$w_s = w_{s,0} \left\langle 1 - \frac{\langle c_{\text{bed}} \rangle}{c_{\text{gel}}} \right\rangle^5. \tag{3}$$

Hence, w_s does not vary on the tidal time scale and is depth uniform. For concentrations much lower than the gelling concentration c_{gel}, w_s equals the prescribed clear-water settling velocity $w_{s,0}$.

The third and final extension to the model is a dependency between the eddy viscosity, eddy diffusivity, and bed friction parameter and the sediment concentration, parametrizing the effects of sediment-induced turbulence damping. The eddy viscosity and eddy diffusivity are assumed to be constant over a tidal cycle and are depth uniform. They are parametrized as functions of the depth-averaged velocity $U(x,t)$, the depth (consisting of the bed level H, reference surface level R, and surface elevation ζ), and the depth-averaged gradient Richardson number $\overline{\text{Ri}}(x,t)$

$$A_v = \left\langle c_{v,1}(z_0^*) U (H + R + \zeta) F(\overline{Ri}) \right\rangle, \tag{4}$$

$$K_v = \left\langle \frac{c_{v,1}(z_0^*)}{\sigma_\rho} U(H + R + \zeta)G(\overline{Ri}) \right\rangle. \tag{5}$$

The coefficient $c_{v,1}$ is a drag coefficient that depends on a dimensionless roughness height $z_0^* = \frac{z_0}{H}$ (Dijkstra et al., 2017), and σ_ρ is the Prandtl-Schmidt number, which is set to 1 by default. The functions F and G are based on the damping functions suggested by Munk and Anderson (1948), using the depth-averaged Richardson number $\overline{Ri}$ instead of the bulk Richardson number. The damping functions read

$$F(\overline{Ri}) = \left(1 + 10\overline{Ri}\right)^{-1/2}, \tag{6}$$

$$G(\overline{Ri}) = \left(1 + 3.33\overline{Ri}\right)^{-3/2}, \tag{7}$$

with the gradient Richardson number defined as

$$Ri = -\frac{g\beta_c}{\rho_0} \frac{c_z}{u_z^2 + u_{z,\min}^2}.$$

Here $\beta_c = 1 - \rho_0/\rho_s$ is the conversion factor from sediment concentration to density, where ρ_0 is the clear-water density (assumed equal to 1,000 kg/m³) and ρ_s is the dry sediment density (assumed equal to 2,650 kg/m³). The variable u_z is the vertical gradient of the along-channel velocity, and $u_{z,\min}$ represents a background shear to parametrize flows that are not accounted for (e.g., lateral flows, wind-driven flow, and small-scale circulations), nonlocal turbulence production and inertia in turbulence dissipation. Practically, it prevents the Richardson number from becoming unrealistically large.

The bed shear stress used to compute the friction felt by the water motion, $\tau_{b,w}$, is parametrized using an expression that captures the qualitative effect of a quadratic friction law

$$\tau_{b,w} = s_f u_{\text{bed}}, \tag{8}$$

where u_{bed} is the velocity near the bed and s_f is a partial slip parameter that depends on the depth-averaged velocity U, defined as (Dijkstra et al., 2017)

$$s_f = \left\langle c_{v,2}(z_0^*)c_D U \right\rangle. \tag{9}$$

The function $c_{v,2}$ is a drag coefficient that depends on z_0^* and c_D is a reduced-drag coefficient, which accounts for the deformation of the logarithmic boundary layer due to sediment stratification. As the model does not resolve the bottom-most part of this boundary layer, the deformation of this boundary layer needs to be accounted for in the bed friction parametrization. This is done through a reduced-drag coefficient following studies by Adams and Weatherly (1981), Friedrichs et al. (2000), and Wang (2002). This reduced-drag coefficient is expressed as

$$c_D = \left(1 + A \left\langle Rf_{\text{bed}} \right\rangle\right)^{-2}, \tag{10}$$

with the parameter A empirically determined by the aforementioned studies and set to 5.5. The parameter Rf_{bed} is the flux Richardson number near the bed, which reads

$$Rf_{\text{bed}} = \frac{K_v}{A_v} Ri_{\text{bed}}.$$

To avoid a drag reduction that is much stronger than has been observed in laboratory studies, the value of Rf_{bed} is limited to a maximum value $Rf_{\max} = 2$. A flux Richardson number of 2 may still seem large compared to the often mentioned critical value around 0.25. However, the Richardson number must be interpreted differently in this model, as our turbulence model does not produce a sudden strong reduction of turbulent mixing at Richardson numbers near its theoretical critical value. As a result the model allows for much larger Richardson numbers.

Whereas the bed shear stress for the water motion parametrizes the friction generated in the lowest part of the bottom boundary layer, the bed shear stress that generated sediment erosion τ_b strictly applies to the
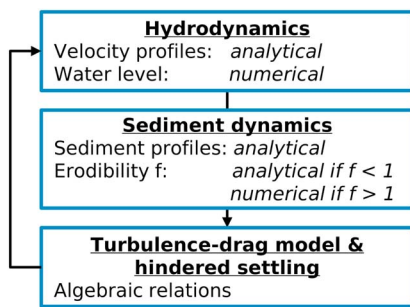
Figure 2. Summary of the model components (boxes) and the solution methods (in italics), indicating the iteration over the components by arrows.

water-bed interface. Therefore, near-bed stratification should not be accounted for in the bottom boundary condition for sediment. Therefore, τ_b, used in the erosion formulation 2, is parametrized as

$$\tau_b = s_s u_{\text{bed}}, \tag{11}$$

where s_s is equal to s_f with $c_D = 1$.

The use of a depth-averaged and tidally averaged eddy viscosity, eddy diffusivity, and settling velocity, combined with the iFlow solution procedure (Dijkstra et al., 2017), allows for semianalytical solutions to the hydrodynamic and sediment concentration equations. The solution procedure is summarized in the flow diagram of Figure 2. Given the turbulence and drag parameters, the vertical profiles of the velocity are computed analytically. They still depend on the water levels, which are computed numerically. The water motion is used as input to the sediment dynamics, where the vertical variation of the sediment concentration is computed analytically and depends on the erodibility f. The erodibility is computed analytically if $f < 1$ everywhere and numerically otherwise. Using the sediment concentrations, new values for the settling velocity (equation (3)), turbulence, and drag parameters (equations (4), (5), and (9)) are obtained. This is iterated until the settling velocity and turbulence parameters have a relative change per iteration of less than 10^{-4}. For the numerical computation of the water level and erodibility, a second-order finite differences method is used on an equidistant grid containing 250 grid cells.

3. The Ems in 1965 and 2005

The Ems River Estuary consists of the lower Ems estuary on the Dutch-German border, the shallow Dollard Bay, the upper Ems estuary, and tidal river in Germany. Following earlier studies by Chernetsky et al. (2010) and Van Maren et al. (2015), we focus on the upper estuary and tidal river; see Figure 1. This part of the river stretches from Knock to a tidal weir at Herbrum and has a total length of 64 km.

The width of the estuary is estimated from satellite images and is fitted by a smooth polynomial curve; see Figure 3 (left panel). Shallow areas and the Dollard bay have been ignored. It is assumed that the width is the same between 1965 and 2005, because most of the narrowing works and land reclamations were done before 1965. The depth of the channel in 1965 is derived from Janssen (1968); see also De Jonge et al. (2014). Channel depth data for 2005 were obtained from WSA Emden and were presented earlier by De Jonge et al. (2014). Both sets of depth measurements and smooth curve fits for use in the model are plotted in Figure 3 (right panel). The smooth fits average over the large-scale dunes with typical amplitudes of 2–3 m and lengths of 5–10 km. Hence, the model does not resolve their effect on the dynamics of the water and sediment.

Observed water levels are used to determine the tidal forcing at the seaward boundary in the model, to calibrate the 1965 model and to validate the results of the 2005 model. For 1965, the observed water level
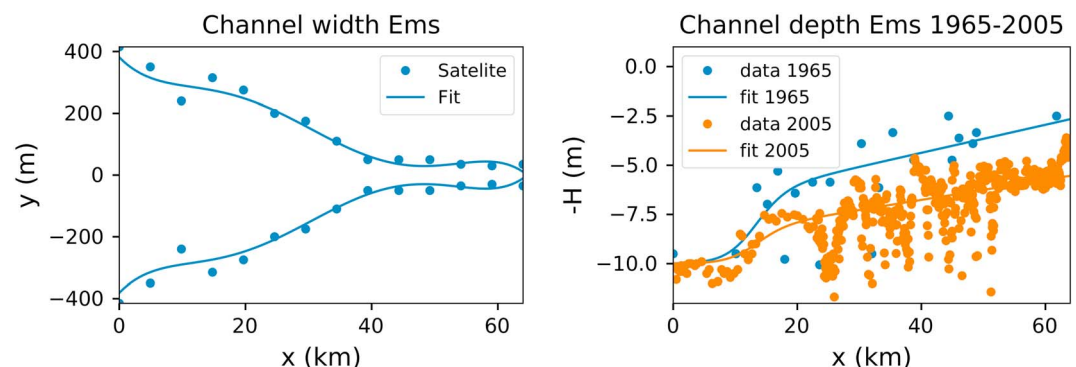

Figure 3. (left) Channel width estimated from satellite images and a smooth fit used in the model. (right) Measured channel depth in 1965 (Janssen, 1968) and 2005 (WSA Emden; see also De Jonge et al., 2014) with smooth fits used in the model.

Table 1
Default Model Parameters for the Ems in 1965 and 2005

Component	Parameter	Description	1965	2005
Hydrodynamics	A^0	M_2 water level amplitude at $x = 0$	1.34 m	1.40 m
	A^1	M_4 water level amplitude at $x = 0$	0.18 m	0.21 m
	ϕ^0	M_2 water level phase at $x = 0$	0	0
	ϕ^1	M_4 water level phase at $x = 0$	$-178°$	$-171°$
	Q	River discharge	30–150 m³/s	
Salinity	s_{sea}	Seaward salinity	30 psu	
	x_c	Translation (depends on Q)	4.9 to -4.2 km	
	x_l	Salt intrusion length scale (depends on $4Q4$)	13.5 to 10.4 km	
Sediment	c_{sea}	depth-averaged subtidal concentration at $x = 0$	0.1 kg/m³	
	K_h	Horizontal eddy diffusivity	100 m²/s	
	M	Erosion parameter	0.02 s/m	
	$w_{s,0}$	Clear-water settling velocity	1 mm/s	
	c_{gel}	Gelling concentration	100 kg/m³	
Turbulence	σ_ρ	Prandtl-Schmidt number ($=A_v/K_v$ for $Ri = 0$)	1	
	$u_{z,\text{min}}$	Velocity gradient for background turbulence production	0.03 L/s	

amplitude is derived from tidal curves for a mean tide drawn in a report of the German Federal Waterways Engineering and Research Institute (Bundesanstalt für Wasserbau (BAW), 1967). The M_2 and M_4 tidal amplitudes and relative phases are derived from this by a spectral analysis, but the tidal phase difference between the stations could not be derived. The 2005 data set is available from the Lower Saxony state department for water management, coastal and nature conservation (NLWKN) as a high-resolution time series of almost the entire year. The year-averaged M_2 and M_4 tidal amplitude and phase are derived using complex demodulation (e.g., Jalón-Rojas et al., 2016), thereby averaging over the spring-neap cycle and seasonal variations. From the observations we derive the model forcing at the seaward boundary; see Table 1.

The river discharge of the Ems River is measured at Versen, a station approximately 40 km upstream from the weir at Herbrum. Taking the average of daily discharge measurements between 1987 and 2006, we find a year-averaged discharge of 80 m³/s, a summer-averaged (July–September) discharge of 40 m³/s and a winter-averaged (January–March) discharge of 150 m³/s. It is assumed that the average discharge remained the same between 1965 and 2005. At Leer (km 36), the river Leda enters the Ems. This river has a small but significant discharge but is neglected in this study.

Following Talke, De Swart, and De Jonge (2009), we assume that the salinity is well mixed and may be described diagnostically by a hyperbolic tangent profile. The length of the salt intrusion and salinity at the mouth depend on the discharge (see Table 1 in Talke, De Swart, and De Jonge, 2009). The salinity profile reads

$$s = \frac{s_{\text{sea}}}{2} \left(1 - \tanh\left(\frac{x - x_c}{x_L} \right) \right), \tag{12}$$

where $s_{\text{sea}} = 30$ psu. For year-averaged conditions, $x_c = -3.5$ km and $x_L = 11.5$ km.

We prescribe a depth-averaged subtidal suspended sediment concentration of 0.1 kg/m³ at the seaward boundary (Talke, De Swart, & Schuttelaars, 2009) and assume that this has not changed between 1965 and 2005. This seems a conservative estimate, as the concentration has likely increased in the lower Ems Estuary after 1965 (De Jonge et al., 2014). We choose a horizontal eddy diffusivity $K_h = 100$ m²/s and have verified that the model results are insensitive to the exact value of this parameter. For the gelling concentration we choose a default value of 100 kg/m³. For the settling velocity, erosion parameter, Prandtl-Schmidt number, and background turbulence production $u_{z,\text{min}}$ we choose default values given in Table 1. The effect of varying these parameter values is demonstrated in section 6. The default setting for the settling velocity $w_{s,0} = 1$ mm/s and the erosion parameter $M = 0.02$ s/m correspond to those used by Van Maren et al. (2015), where our M corresponds to their M/τ_c. The default parameter settings are summarized in Table 1.
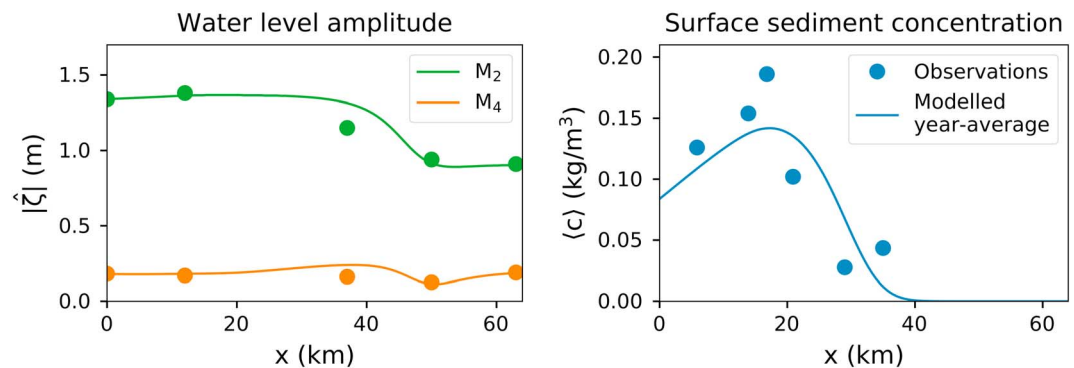
Figure 4. (left) Water level amplitude for 1965 for the two main tidal constituents M_2 and M_4 during year-averaged discharge conditions ($Q = 80$ m^3/s). The lines represent model results. The dots are reported observed water levels under average conditions (Bundesanstalt für Wasserbau, 1967). (right) Subtidal surface sediment concentration in 1965 from the model (blue line) for equilibrium conditions corresponding to year-averaged conditions. The model results are compared to the year average of observations from 1954 presented by De Jonge et al. (2014). Note that the number of observations in 1954 is very limited.

4. Model Calibration and Results

4.1. Model Calibration

The 1965 model with the default parameter settings (Table 1) and year-averaged discharge ($Q = 80$ m^3/s) is calibrated against the M_2 water level amplitude measurements, resulting in an optimal value of the dimensionless roughness height of $z_0^* = 0.0093$. The resulting water level amplitudes of the two main tidal constituents are plotted in Figure 4 (left panel). As the 1965 modeled M_2 water level is calibrated to the measurements, it is to be expected that this yields good correspondence. Also the M_4 tide in 1965 corresponds well to the measurements, giving confidence that the most important hydrodynamic processes are captured.

Little data are available for calibrating the sediment concentrations in 1965. Therefore, parameter values in the sediment model ($w_{s,0}$, c_{sea}, and M) are not calibrated to best fit the measurements but are based on previous studies. As an indication of the fit between model and observations, we have used data from 1954 presented by De Jonge et al. (2014), which are supposed to represent yearly mean surface concentrations, but the exact conditions under which they were obtained are unknown. The data show an ETM around km 20 with maximum surface sediment concentrations around 0.2 kg/m^3 (see Figure 4, right panel). The model results show a similar location of the ETM and magnitude of the surface concentration compared to the observations.

The parameter values are fixed for all discharge values and used for both the 1965 and 2005 cases. The model is thus *not* recalibrated for the 2005 case. The 2005 case therefore only differs from the 1965 case by the level of the bed and some minor changes to the M_2 and M_4 tidal amplitude and phase at the mouth to make it easier to compare to measurements. It has been verified that the changes to the forcing at the mouth have a negligible influence on the results (see supporting information). Below we discuss the results of both cases for various discharge conditions.

4.2. Results for a Low River Discharge

First, focussing on the average summer river discharge of $Q = 40$ m^3/s, the water level amplitude and phase for both 1965 and 2005 are plotted in Figure 5. The water level for the 1965 case is almost the same as in Figure 4 for the year-averaged river discharge. This is because the river-induced velocity is much smaller than the tidal velocity and the sediment concentration has little influence on the damping of turbulence in this case. The 2005 M_2 water level shows strong amplification compared to 1965 and the tidal wave travels faster through the estuary (i.e., smaller phase difference between the mouth and the weir). This observation is consistent with earlier modeling studies by, e.g., Chernetsky et al. (2010) and Winterwerp et al. (2013). However, the amplification and the wave celerity of the M_2 tide seem to be slightly overestimated. Observations indicate that the M_4 water level amplitude has amplified as well and that the M_4 tidal wave travels faster through the estuary. This is reproduced but overestimated by the model.

Concerning the flow velocity (middle-left panel), the cross-sectionally averaged M_2 flow velocity has only increased by at most 20% between 1965 and 2005. The M_4 flow velocity on the other hand has increased by
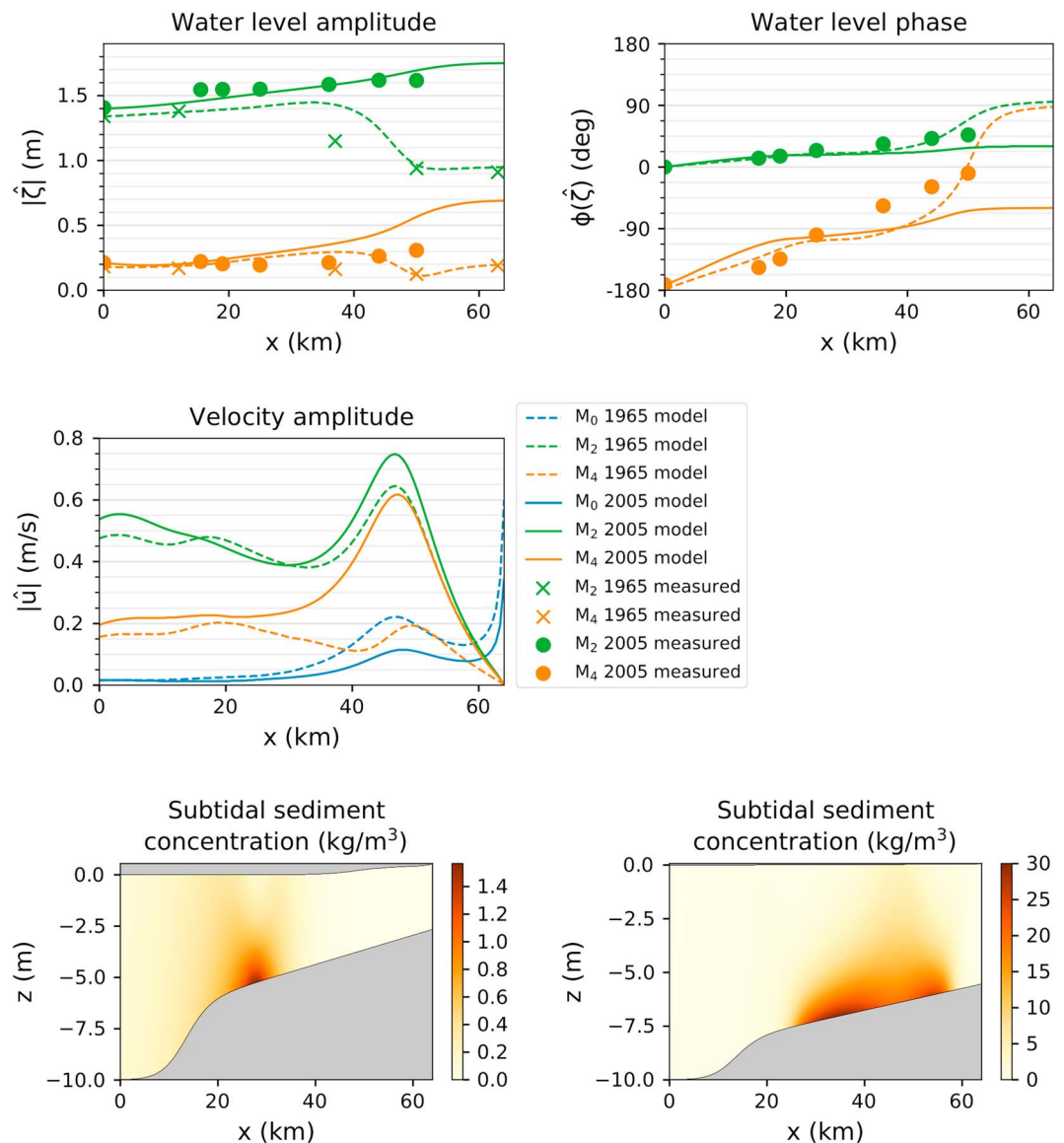
Figure 5. Model results for the 1965 and 2005 cases with summer average discharge, $Q = 40 \text{ m}^3/\text{s}$.

more than 100% between 1965 and 2005 in the area between 40 and 60 km. Additionally, the subtidal (i.e., M_0) velocity has decreased in this area by up to 40%.

The modeled subtidal sediment concentration in 1965 is plotted in the lower-left panel. It shows that the ETM is located around km 25 in 1965, with concentrations of up to 1.5 kg/m^3 near the bed and concentrations under 0.3 kg/m^3 at the surface. The relatively large difference between bottom and surface concentrations is related to sediment-induced turbulence damping in the ETM, which keeps the sediment confined to the bed. As the ETM remains narrow, this damping of turbulence acts locally and thus has a negligible effect on the water motion. The order of magnitude of the near-bed concentration of 1.5 kg/m^3 seems realistic in comparison to observations of 1–2 kg/m^3 near the bed between Emden (km 10) and Terborg (km 26) in 1949 reported by Dechend (1950).

In the 2005 case (lower-right panel), the ETM became wide, covering an area between km 25 and 60. Near-bed concentrations increased up to 30 kg/m^3. Concentrations at the surface range from 1 to 4 kg/m^3 between km 35 and 60. These results capture the qualitative characteristics of the observed ETM; observations made by Talke, De Swart, and Schuttelaars (2009) during one cruise in 2006 show sediment concentrations near the bed of 10–30 kg/m^3 and near the surface of approximately 1 kg/m^3 in the entire
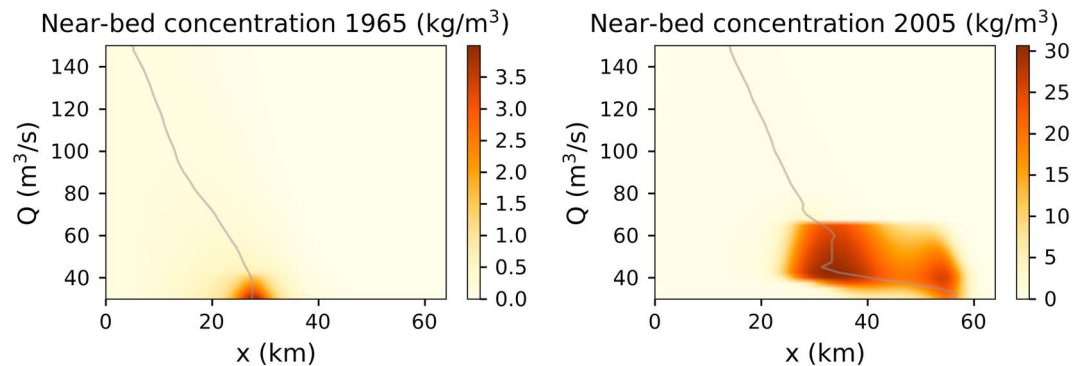
Figure 6. Near-bed modeled sediment concentration along the channel (horizontal axis) for a various long-term constant discharge values (vertical axis) for the 1965 and 2005 cases. The gray line indicates the location of the estuarine turbidity maximum.

zone between km 35 and 60. Similar or higher near-bed concentrations and fluid mud have been observed by Wang (2010), Papenmeier et al. (2013), Winterwerp et al. (2017), and Becker et al. (2018). De Jonge et al. (2014) reports observed surface concentrations locally exceeding 3 kg/m^3.

Comparing the modeled concentrations between 1965 and 2005, the maximum near-bed concentration in the domain has gone up by a factor of 20, while the maximum near-surface concentration has increased by a factor of 14. The amount of sediment suspended in the estuary, in the model, has increased by a factor of 8 from approximately 40 to 300 million kg.

4.3. Sensitivity to the River Discharge

The sensitivity of the model results to the river discharge is investigated by varying the discharge between 30 and 150 m^3/s. In each experiment, the discharge is assumed to be constant and the resulting water motion and sediment concentration are in dynamic equilibrium. Figure 6 shows the resulting near-bed suspended sediment concentration as a function of the along-channel distance (horizontal axis) and the river discharge (vertical axis). The gray line in the figures indicates the location of the maximum near-bed concentration in the ETM.

In 1965 the ETM is narrow and located around km 25–30 for discharges below 60 m^3/s. At these low discharges, near-bed concentrations of several kilograms per cubic meter occur, which correspond to surface concentrations around 0.2–0.4 kg/m^3. For a discharges below 30 m^3/s, concentrations are locally up to 4 kg/m^3 near the bed. It is unlikely that such conditions were ever attained, as such discharges only occurred for 10% of the time. For discharges exceeding 70 m^3/s, the ETM moves downstream and the maximum near-bed concentration rapidly decreases below 1 kg/m^3. The M_2 and M_4 water level elevation (not shown) is almost independent of the river discharge.

In 2005 we find a wide ETM with high concentrations exceeding 30 kg/m^3 for discharges between 35 and 70 m^3/s. For lower discharges, we also find high concentrations but more concentrated at the landward side of the estuary. Conditions with discharges below 70 m^3/s occur approximately 60% of the time with uninterrupted periods of several months each year, making it is probable that such concentrations could indeed be attained. For discharges above 70 m^3/s (approximately 40% of the time) the high concentrations disappear and only a narrow ETM with much lower concentrations remains. For these high discharges, concentrations are only marginally higher than for the same discharge conditions in 1965. Additionally, the tidal amplification is much less than in Figure 5. Although observations of sediment concentrations show a marked decrease of the suspended sediment concentration at high river discharge (Winterwerp et al., 2017), the modeled concentrations are much lower than observed. The modeled reduction in tidal amplification is not observed. The model therefore does not seem to capture the observed characteristics of the water motion and sediment dynamics at $Q > 70$ m^3/s.

The results show that the transition from a narrow ETM with relatively low concentrations in 1965 to a wide ETM with much higher concentrations in 2005 may be reproduced by only increasing the channel depth for long-term discharges below 70 m^3/s. The model does not reproduce the transition if the discharge is higher; see section 7 for a more detailed discussion of this.
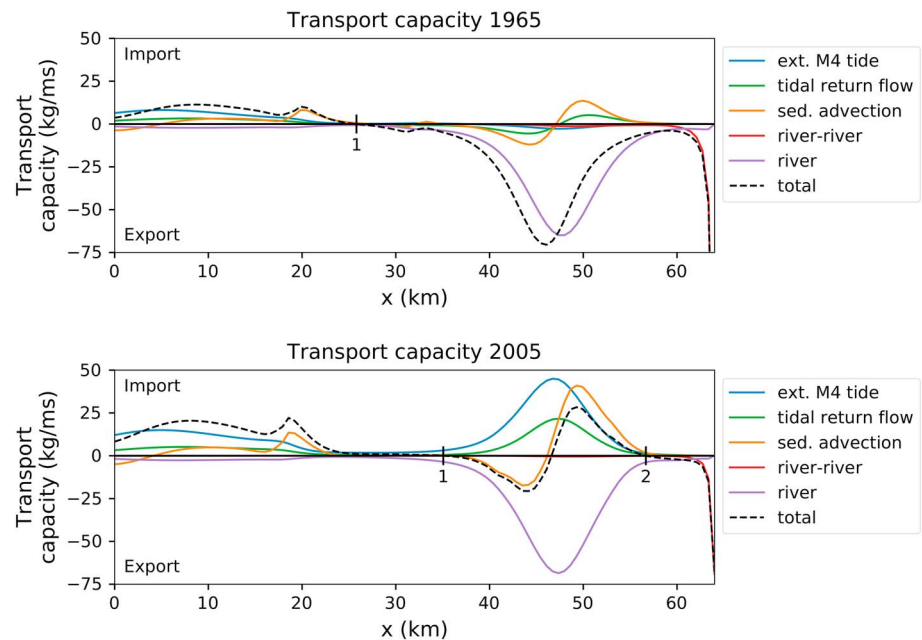
Figure 7. Sediment transport capacity per meter width (and integrated over depth) for 1965 (top) and 2005 (bottom) for summer average discharge conditions ($Q = 40$ m^3/s). The five most important contributions to the transport capacity are plotted, as well as the sum of all modeled contributions (black dashed line). Downward sloping zero crossings of the total transport capacity indicate a convergence zone and are marked by a vertical line and number.

5. Analysis of the Results

We will look closer at the physical processes that allow for the transition from moderate concentrations in 1965 to high concentrations in a wide ETM in 2005 for discharges below 70 m^3/s. We consider two aspects

1. *Sediment trapping (along-channel processes).* The amount of sediment that can be contained within the estuary by the flow and sediment dynamics.
2. *Local resuspension (vertical processes).* The amount of sediment that can potentially be brought into suspension given the erosion properties of the bed and the strength of the flow.

These aspects are discussed separately in sections 5.1 and 5.2.

5.1. Sediment Trapping

In order to analyze the processes resulting in sediment trapping, we will look at the various contributions to the suspended sediment transport. The suspended sediment transport $\mathcal{T}$ is written as the sum of the advective and diffusive transport integrated over the cross-section, that is,

$$\mathcal{T} = \left\langle B \int_{-H}^{R+\zeta} uc - K_h c_x \, dz \right\rangle, \tag{13}$$

where B is the width, u is the along-channel velocity, c is the sediment concentration, c_x is the along-channel sediment concentration gradient, and K_h is the prescribed horizontal eddy diffusivity (see Table 1). Between 1965 and 2005, the flow velocity, sediment concentration, and location of the ETM have changed (e.g. see Figure 5). Hence, there are so many differences in the sediment transport in 1965 and 2005 that a comparison of the sediment transport processes between the years does not give much insight.

To overcome this problem, we look at the *the transport capacity*: the sediment transport $\mathcal{T}$ that would occur if there were an abundance of sediment on the bed everywhere in the estuary (i.e., $f = 1$ everywhere) given the modeled hydrodynamic conditions (flow velocity and turbulence field) and sediment parameters (effective settling velocity and erosion parameter). A formal mathematical definition is given in Appendix A. The transport capacity shows the tidally averaged initial redistribution of a uniform layer of sediment on the bed. Unlike the total sediment transport, the transport capacity depends mainly on the hydrodynamic conditions and sediment parameters and only indirectly on the location of the ETM and magnitude of the sediment concentration. As a result, the comparison between results of 1965 and 2005 is not complicated
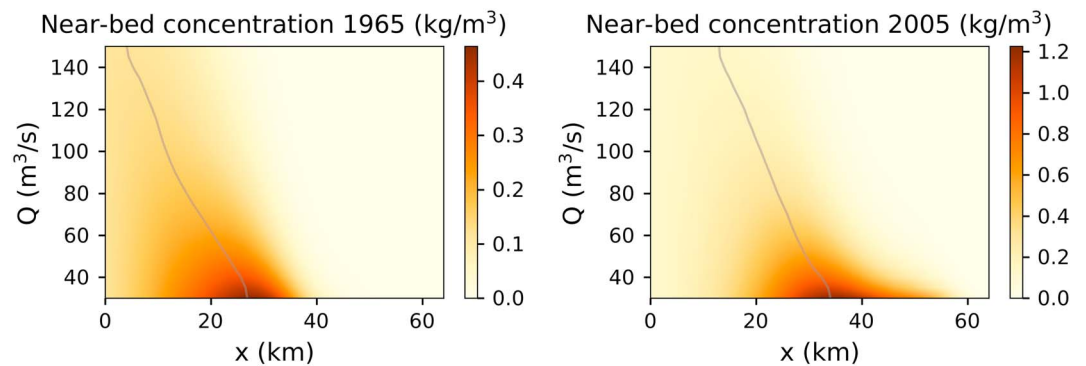
Figure 8. Near-bed modeled sediment concentration along the channel (horizontal axis) for a various long-term constant discharge values (vertical axis) for the 1965 and 2005 cases without sediment-induced reduction of the bed roughness, eddy viscosity and eddy diffusivity. Sediment concentrations are much lower than in Figure 6 with sediment-induced turbulence damping and no strong transition is observed between 1965 and 2005.

by the changed location of the ETM and large increase in sediment concentration and gives more insight. Furthermore, the transport capacity gives information about the trapping locations, because the convergence and divergence points of the transport capacity (i.e., locations where the transport capacity is zero) correspond to the maxima and minima in f.

5.1.1. Contributions to the Transport Capacity

iFlow distinguishes several contributions to the transport capacity related to different physical mechanisms. The five most important contributions for the 1965 and 2005 cases are plotted in Figure 7. Before comparing the transport capacities between the years, we introduce the physical mechanisms of these contributions are related to the following:

- The *external M_4 tide* contribution is due to tidal asymmetry caused by the M_2 tide and M_4 tide entering the estuary at the mouth. This contribution to the M_4 tide is generated outside the estuary on the shallow shelf and propagates through the estuary, causing asymmetry in the velocity during ebb and flood and therefore net sediment transport.
- The *tidal return flow* contribution is the transport capacity due to Stokes drift and the corresponding return flow. The Stokes drift is associated with sediment import. At least partly compensating this import, the return flow velocity contains a subtidal contribution which typically causes export of sediment. Additionally, the return flow velocity has an M_4 contribution, which may cause import or export of sediment, depending on the phase-lag with the M_2 tide.
- The *sediment advection* contribution represents the transport due to spatial settling lag (see, e.g., De Swart & Zimmerman, 2009; Van Straaten & Kuenen, 1957). This contribution tends to transport sediment toward along-channel minima in the tidal velocity amplitude.
- The *river* contribution consists of two parts: the river-induced flushing of tidally resuspended sediment and the transport due to the tidal asymmetry caused by the tide-river interaction. Both contributions cause an export of sediment
- The *river-river* contribution represents the river-induced flushing of sediment resuspended by the river flow. This contribution is therefore independent of the tide and causes sediment export close to the landward boundary, where the river-induced flow dominates over the tidal flow.

5.1.2. Comparison of the Transport Capacity in 1965 and 2005

In 1965 and 2005 the total transport capacity (black dashed lines in Figure 7) is positive (i.e., directed upstream) in the first 25 and 35 km, respectively, and negative (i.e., directed downstream) from there to km 45. This convergence leads to the development of an ETM around km 25 and 35 (number 1 in the figure). In 1965, the transport capacity is negative upstream from km 45. In 2005, however, the transport capacity is positive between km 45 and 57, leading to a second convergence zone around km 57 (number 2 in the figure). These two trapping zones appear as one large ETM zone stretching from km 25 to 60.

The dominant exporting transport contribution in both years is the river discharge. Import is mainly caused by the contributions due to the external M_4 tide and tidal return flow (see section 5.1.1). The most important difference between 1965 and 2005 is the large increase of these importing contributions between km 35 and 57. This increase is related to the increase in the M_4 velocity amplitude (c.f. Figure 5). In addition, the phase

Table 2
Computed Resonance Lengths for the M_2 and M_4 Tide in the Cases of 1965 and 2005 for a Friction Parameter Calibrated for 1965 and 2005

Case	Resonance length	
	M_2 tide	M_4 tide
1965	39 km	37 km
2005 with friction as in 1965	55 km	51 km
2005 with friction as in 2005	72 km	63 km

Note. A resonance length close to the actual length of 64 km indicates that the tidal amplitude is very sensitive to changes in depth or friction.

difference between the M_2 tidal velocity and erosion asymmetry due to the external M_4 tide and M_4 tidal return flow has become more favorable for import (not shown).

5.1.3. Role of Sediment-Induced Turbulence Damping

The strong effect of sediment-induced turbulence damping in the Ems cannot be captured in a specific contribution to the transport capacity, because it is strongly and mutually dependent on the flow and sediment concentration. To capture the effect of sediment-induced damping on the sediment trapping, we therefore compare results with and without it. Sediment-induced damping is turned off by setting F, G, and c_D in equations (4), (5), and (10) equal to 1.

Figure 8 shows the resulting maximum near-bed concentration along the channel versus the river discharge. This shows moderate sediment concentrations, with concentrations not exceeding 1.2 kg/m^3 even for a low discharge of 30 m^3/s. Compared to 1965, the maximum sediment concentrations in 2005 are higher and the ETM is found more upstream. However, the level of the sediment concentration in 2005 and the changes between 1965 and 2005 are much smaller than in the case with sediment-induced turbulence damping (cf. Figure 6). Without sediment-induced turbulence damping, concentrations remain moderate and the observed transition in sediment concentration between 1965 and 2005 is not reproduced. The sediment-induced damping of turbulence is separated further into the effects of damping of the eddy viscosity, eddy diffusivity, and bed friction in the supporting information, showing that damping in all parameters is important.

5.1.4. Resonance

The previous sections demonstrate that the increase in the M_4 tidal velocity amplitude in combination with sediment-induced turbulence damping is essential for the increase in sediment concentrations between 1965 and 2005. The reason that this effect is so strong is better explained by looking at the resonance characteristics. Resonance is a state of maximum tidal amplification. Hence, when an estuary is close to resonance, the water level amplitude becomes very sensitive to changes in the characteristics of the estuary. Here we will take this as a proxy for sensitivity of the tidal velocity amplitude as well. Whether an estuary is in resonance depends on various parameters including the depth, friction (i.e., effect of eddy viscosity and bed friction), and length and is furthermore different for each tidal constituent.

We take the depth and friction of the Ems estuary in 1965 and 2005 and derive the length at which the estuary would be in resonance for the M_2 and M_4 tide, that is, the *resonance length*. This is done on the basis of a simple one-dimensional hydrodynamic model for the linear wave propagation of the externally forced M_2 and M_4 tide (see, e.g., Friedrichs, 2010). Results are summarized in Table 2.

In 1965, we find a resonance length of 39 and 37 km for the M_2 and M_4 tide, respectively. This is very short, because the estuary is strongly friction dominated; the tide becomes damped by friction for larger length. When deepening the estuary to 2005 depth, but keeping friction as in 1965, the resonance length increases, explaining part of the amplification of the M_2 and M_4 tide between 1965 and 2005. When also changing the friction to 2005 conditions, representing the sediment-induced damping of turbulence, the resonance length increases further. The resonance length for the M_2 tide increases beyond the actual length of the estuary. Hence, the M_2 is not closer to resonance than with the 2005 depth and 1965 friction. Nevertheless, the M_2 tide amplifies somewhat more because of the reduced friction. The transport contribution due to the tidal return flow is related to the M_2 tide and is larger because of the amplification of this M_2 tide. The resonance length of the M_4 tide on the other hand is very close to resonance. It therefore amplifies not only because of
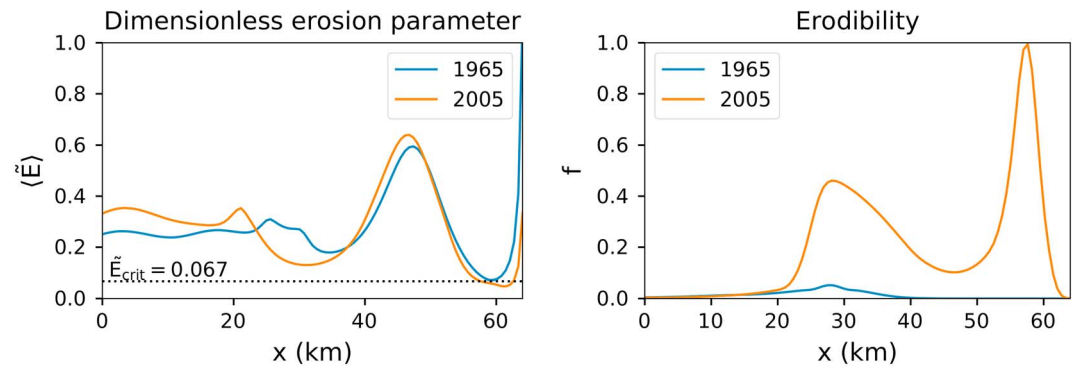
Figure 9. Dimensionless erosion parameter $\tilde{E}$ and erodibility f for 1965 and 2005 with average summer discharge ($Q = 40$ m^3/s). (left) The dimensionless erosion parameter (See equation (14)) and its threshold value 0.067. If $\langle \tilde{E} \rangle$ exceeds the threshold, local resuspension does not restrict the maximum suspended sediment concentration. (right) The erodibility f, which is a measure for the availability of easily erodible sediment. A value $f < 1$ indicates that sediment availability is limiting the sediment concentration, while $f = 1$ indicates that local resuspension is limiting the sediment concentration.

the reduced friction but also because of resonance. The transport contribution due to the external M_4 tide has therefore become much larger.

5.2. Local Resuspension Criterion

The second aspect important for understanding the dynamics of the suspended sediment concentration is the ability of the flow to keep sediment in suspension by erosion or resuspension. Dijkstra et al. (2018) derived that the maximum concentration that may be locally resuspended is related to a dimensionless erosion parameter $\tilde{E}$. For our erosion formulation (equation (2)), this parameter is expressed as

$$\tilde{E} = \frac{M|\tau_b|}{w_{s,0}c_{\text{gel}}}. \tag{14}$$

Using the hindered settling parametrization of equation (3), the maximum concentration is limited to a value that depends on the tidally averaged dimensionless erosion parameter $\langle \tilde{E} \rangle$ if $\langle \tilde{E} \rangle$ is smaller than a threshold value of 0.067 (see Dijkstra et al., 2018, for details). This maximum cannot exceed 16% of the gelling concentration, that is, 16 kg/m^3 in our case. If $\langle \tilde{E} \rangle > 0.067$, there is no restriction to the concentration that can be maintained by resuspension. This is because of a positive feedback, where hindered settling leads to reduced deposition rates and hence a larger net erosion (=erosion-deposition).

Figure 9 (left panel) shows $\langle \tilde{E} \rangle$ for the 1965 and 2005 cases for the average summer discharge, together with the threshold value. The tidally averaged dimensionless erosion parameter is well over the threshold in most of the domain. In those locations, all the available sediment is resuspended at least during some part of the tide. Only in 2005 between 59 and 62 km does $\langle \tilde{E} \rangle$ drop below the threshold value, where it may restrict the maximum concentration.

Whether the maximum sediment concentration is indeed restricted by local resuspension follows from the erodibility; see Figure 9 (right panel). If $f < 1$ everywhere in the estuary, it is said that the estuary is in an *availability* (or *supply*) *limited* state and the concentration is limited by the amount of sediment trapping. A value $f = 1$ indicates that some easily erodible sediment remains on the bed during the entire tidal cycle and local re-suspension is limiting there. This state is called *erosion* (or *erosion rate*) *limited*. In an erosion-limited state, the estuary imports sediment, which is deposited in the area where $f = 1$, leading to a growing bottom pool (Brouwer et al., 2018). Since the local growing bottom pool acts as a sediment sink, even a small area with $f = 1$ leads to lower concentrations in equilibrium elsewhere in the estuary. The figure shows that $f < 1$ along the entire estuary in both years, although only marginally in 2005. Hence, it is concluded that sediment trapping is the limiting mechanism, even in the small area between km 59 and 62 in 2005, where sediment re-suspension could theoretically be limiting.

6. Sensitivity

To explore the robustness of the results to different parameter choices, we present the effect of choosing different values for the clear-water settling velocity and erosion parameter, which are two of the least
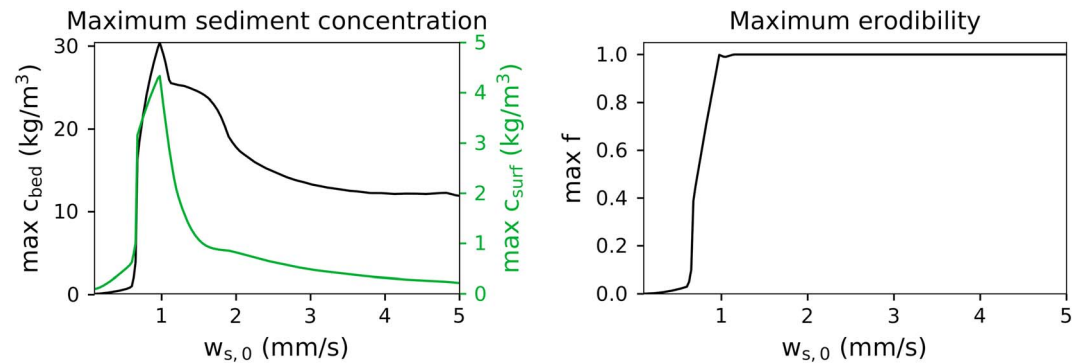
Figure 10. Sensitivity of the model results in 2005 with average summer discharge ($Q = 40$ m^3/s) to the clear-water settling velocity. (left) Subtidal near-bed (black) and surface (green) concentration. (right) Erodibility.

constrained parameters in the model. The sensitivity to two other uncertain parameters, $u_{z,\mathrm{min}}$ and σ_ρ, is demonstrated in the supporting information.

6.1. Sensitivity to the Settling Velocity

To test the sensitivity of the model results to the clear-water settling velocity, $w_{s,0}$ is varied between 0.1 to 5 mm/s. The resulting maximum near-bed and surface concentrations in 2005 are shown in Figure 10, using the default settings for 2005 for all other parameters (see Table 1) and using the average summer discharge of 40 m^3/s. The maximum concentration is small for settling velocities below 0.5 mm/s. At such settling velocities, the sediment behaves like a wash load and will not be trapped inside the estuary. Hence, sediment trapping is limiting the sediment concentration. This is confirmed in Figure 10 (right panel), which shows that $f < 1$ everywhere in the estuary if $w_{s,0} < 0.5$ mm/s. Around $w_{s,0} = 0.5$ mm/s, a sharp transition to high sediment concentrations is found due to the strong feedback effect of sediment-induced turbulence damping. For $w_{s,0}$ between 0.5 and 1 mm/s, the maximum concentration increases with $w_{s,0}$. Sediment trapping is still limiting, but more sediment is trapped as the settling velocity increases. The maximum concentration decreases again if the settling velocity exceeds 1 mm/s. As shown in Figure 10 (right panel), this is because local resuspension becomes limiting ($f = 1$), as the dimensionless erosion parameter $\tilde{E}$ decreases with increasing $w_{s,0}$ by definition (see equation (14)). Under these erosion-limited conditions, sediment deposits at the edges of the wide ETM zone near km 60 and 30 and forms two growing pools of sediment.

6.2. Sensitivity to the Erosion Parameter

The dimensionless erosion parameter $\tilde{E}$ is linearly proportional to the erosion parameter M (equation (14). Hence, the estuary becomes erosion limited at small values of the erosion parameter $\tilde{E}$. If the ETM location remains the same for different values of M, the maximum concentration scales linearly with M. When M becomes sufficiently large so that the estuary becomes supply limited, the maximum concentration is independent of M. At what value of M this occurs depends on the conditions.
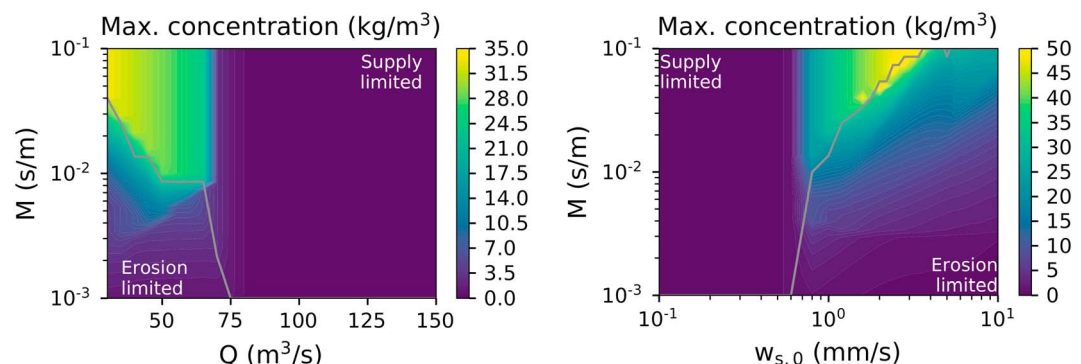

Figure 11. Sensitivity of the near-bed subtidal sediment concentration in the 2005 case to M, Q and $w_{s,0}$. The gray line marks the transition between erosion and supply limited conditions.

Model results obtained by varying both the erosion parameter and the river discharge are presented in Figure 11 (left panel). The gray line indicates the transition point between erosion and supply limited conditions. For each value of the river discharge, the concentration increases with increasing M up to the point where the estuary becomes supply limited and the concentration becomes independent of M. The figure shows high concentrations in the upper-left corner, that is, for high erosion parameters and low river discharges. If the river discharge is high, the sediment trapping is too weak to attain high sediment concentrations regardless of the value of M.

Results of a sensitivity study over the clear-water settling velocity and the erosion parameter for fixed discharge $Q = 40\,\text{m}^3/\text{s}$ are presented in Figure 11 (right panel). For each value of the settling velocity, we again see that the maximum sediment concentration increases with M up to the point where the estuary becomes supply limited. Additionally, for each value of the erosion parameter, we see that the sediment concentration has a maximum for some value of the settling velocity. For low erosion parameters this maximum occurs for settling velocities around 0.5 mm/s but with low maximum concentrations. For high values of the erosion parameter, the maximum concentrations occur for settling velocities around 2 to 3 mm/s and can attain values up to 50 kg/m^3.

7. Discussion and Conclusions

It is demonstrated that deepening of the channel in the Ems River can indeed be responsible for the transition from low to high sediment concentrations using the width-averaged idealized process-based iFlow model. The model was used to simulate two scenarios representing 1965 and 2005, which only differ in the channel depth. Between 1965 and 2005 we find a strong amplification of the tidal water level, a strong increase in the suspended sediment concentration, an upstream movement, and a widening of the ETM to an area between 25 and 60 km upstream from Knock. These features show good qualitative correspondence to observations. Since the model results represent dynamic equilibrium conditions, we draw conclusions on the long-term change of the state of the estuary, not on the sequence of events and time scale of the changes. As the transition from low to high concentrations is found for discharges below 70 m^3/s, which occur on average 60% of the time, it seems likely that the modeled equilibrium conditions can indeed be attained. Therefore, we are confident that the model provides a good qualitative representation of the physical mechanisms that govern the transition.

The physical mechanisms responsible for the transition to high sediment concentrations are analyzed by analyzing sediment transport and resuspension. It is shown that the most important mechanisms responsible for increased sediment import into the estuary after deepening are amplification of the M_4 tidal velocity and sediment-induced damping of turbulence. The increased M_4 tidal velocity increased the tidal asymmetry leading to more import of sediment. Together with sediment-induced damping of turbulence, this results in a positive feedback thereby confirming the hypothesis of the existence of such a feedback by Winterwerp and Wang (2013). It is furthermore found in this study that the combination of deepening and sediment-induced damping of turbulence brought the M_4 tide close to resonance, hence explaining why the import of sediment is so much stronger after deepening compared to the situation before deepening. It has been assumed that resuspension from the bed is efficient by choosing a high value of the erosion parameter and by including hindered settling in the model. This ensures that all the imported sediment can be kept in suspension by the flow, explaining the increase in suspended sediment concentration.

Once the transition to high sediment concentrations has occurred, the model lacks several physical processes that are essential to describe the sediment dynamics. This shows in the 2005 model results by an overestimation of the M_4 tidal water level amplitude and insufficient vertical structure to capture the observed distinct fluid mud layers (e.g., Becker et al., 2018). Furthermore, while lower sediment concentrations are observed during periods of high discharges (Winterwerp et al., 2017), the strong flushing found in the model for discharges higher than 70 m^3/s does not correspond to the observations. The model therefore lacks mechanisms that retain the fluid mud during periods of high discharges. Possible mechanisms that need to be included for a better description of the 2005 state are a critical shear stress for erosion, multiple sediment fractions, internal dynamics (i.e., the effect of a temporally variable density structure on the eddy viscosity and eddy diffusivity; Becker et al., 2018; Winterwerp et al., 2017), and dynamic effects that resolve the time scale for depleting a bottom pool of sediment (e.g. Schoellhamer, 2011).

The physical mechanisms investigated in this study occur in many estuaries, but their response to deepening is not necessarily the same in other estuaries. The feedback between amplification of the M_4 tidal velocity and sediment-induced turbulence damping relies on the M_4 tide evolving toward resonance and depends on the phase difference between the M_2 tide and M_4 tide, which may be different in other estuaries. Additionally, the M_2–M_4 tidal asymmetry that is essential for sediment transport in the Ems may not be essential in other estuaries. Furthermore, sediment resuspension may be limiting instead of sediment trapping in some other estuaries. Therefore, to establish if a similar transition to high sediment concentrations can occur in another estuary, it needs to be investigated whether sediment transport or resuspension is limiting, what sediment transport processes are important, and how these processes respond to deepening.

Appendix A: Formal Definition of the Transport Capacity

The transport capacity used in section 5 can be formally defined from the sediment transport $\mathcal{T}$. For convenience we repeat equation (13) describing $\mathcal{T}$

$$\mathcal{T} = \left\langle B \int_{-H}^{R+\zeta} uc - K_h c_x \, \mathrm{d}z \right\rangle. \tag{A1}$$

This expression is rewritten using iFlow's approximation of the sediment concentration (see also Brouwer et al., 2018)

$$c = \hat{c}^f f + \hat{c}^{f_x} f_x. \tag{A2}$$

Here f is the erodibility (see section 2), which is a measure between 0 and 1 for the abundance of sediment available at the bed for erosion. The quantity $\hat{c}^f$ is the sediment concentration suspended at capacity conditions. The term *capacity conditions* indicates the maximum concentration that can be supported by the flow, assuming an abundant availability of sediment. Indeed, according to equation (A2), the concentration c equals $\hat{c}^f$ if there is an abundance of sediment, that is, $f = 1$ everywhere (resulting in $f_x = 0$). The quantity $\hat{c}^{f_x}$ represents the along-channel sediment dispersion by tidal advection at capacity conditions. Combining equations (A1) and (A2) yields a new expression for the sediment transport

$$\mathcal{T} = \left\langle B \underbrace{\int_{-H}^{R+\zeta} \left(u\hat{c}^f - K_h \hat{c}_x^f \right) f}_{\text{Transport capacity}} - \left(\hat{c}^{f_x} + K_h \hat{c}^f \right) f_x \, \mathrm{d}z \right\rangle. \tag{A3}$$

The *transport capacity T* is now defined as the first term divided by f, that is,

$$T = \left\langle B \int_{-H}^{R+\zeta} u\hat{c}^f - K_h \hat{c}_x^f \, \mathrm{d}z \right\rangle. \tag{A4}$$

This definition is consistent with the transport function T used by Chernetsky et al. (2010).

References

Adams, C. E., & Weatherly, G. L. (1981). Some effects of suspended sediment stratification on an oceanic bottom boundary layer. *Journal of Geophysical Research*, *86*, 4161–4172.

Bundesanstalt für Wasserbau (1967). Modellversuche für die Ems. Bundesanstalt für Wasserbau, Hamburg, in German.

Becker, M., Maushake, C., & Winter, C. (2018). Observations of mud-induced periodic stratification in a hyperturbid estuary. *Geophysical Research Letters*, *45*, 5461–5469. https://doi.org/10.1029/2018GL077966

Brouwer, R. L., Schramkowski, G. P., Dijkstra, Y. M., & Schuttelaars, H. M. (2018). Time evolution of estuarine turbidity maxima in well-mixed, tidally dominated estuaries: The role of availability- and erosion-limited conditions. *Journal of Physical Oceanography*, *48*, 1629–1650.

Chernetsky, A. S., Schuttelaars, H. M., & Talke, S. A. (2010). The effect of tidal asymmetry and temporal settling lag on sediment trapping in tidal estuaries. *Ocean Dynamics*, *60*, 1219–1241.

Cloern, J. E. (1987). Turbidity as a control on phytoplankton biomass and productivity in estuaries. *Continental Shelf Research*, *7*, 1367–1381.

De Jonge, V. N., Schuttelaars, H. M., Van Beusekom, J. E. E., Talke, S. A., & De Swart, H. E. (2014). The influence of channel deepening on estuarine turbidity levels and dynamics, as exemplified by the Ems estuary. *Estuarine Coastal and Shelf Science*, *139*, 46–59.

De Swart, H. E., & Zimmerman, J. T. F. (2009). Morphodynamics of tidal inlet systems. *Annual Review of Fluid Mechanics*, *41*, 203–229.

Dechend, W. (1950). Die geologischen Untersuchungen in der Ems. WSA Emden, In German.

Dijkstra, Y. M., Brouwer, R. L., Schuttelaars, H. M., & Schramkowski, G. P. (2017). The iFlow modelling framework v2.4. A modular idealized process-based model for flow and transport in estuaries. *Geoscientific Model Development*, *10*, 2691–2713.

Dijkstra, Y. M., Schuttelaars, H. M., & Winterwerp, J. C. (2018). The hyperturbid state of the water column in estuaries and rivers: The importance of hindered settling. *Ocean Dynamics*, *68*, 377–389.

Friedrichs, C. T. (2010). Contemporary issues in estuarine physics. In A. Valle-Levinson (Ed.), *Barotropic tides in channelized estuaries* (pp. 27–61). Cambridge, UK: Cambridge University Press.

Friedrichs, C. T., Wright, L. D., Hepworth, D. A., & Kim, S. C. (2000). Bottom-boundary-layer processes associated with fine sediment accumulation in coastal seas and bays. *Continental Shelf Research*, *20*, 807–841.

Jalón-Rojas, I., Schmidt, S., Sottolichio, A., & Bertier, C. (2016). Tracking the turbidity maximum zone in the Loire Estuary (France) based on a long-term, high-resolution and high-frequency monitoring network. *Continental Shelf Research*, *117*, 1–11. https://doi.org/10.1016/j.csr.2016.01.017

Janssen, T. (1968). Das Elend des Emderfahrwassers und seine Beseitigung. Verlag Ostfriesische Landschaft, Aurich, p.26.

Kandiah, A. (1974). Fundamental aspects of surface erosion of cohesive soils (Ph.D. Thesis), University of California, Davis.

Munk, W. H., & Anderson, E. R. (1948). Notes on a theory of the thermocline. *Journal of Marine Research*, *7*, 276–295.

Papenmeier, S., Schrottke, K., Bartholomä, A., & Flemming, B. W. (2013). Sedimentological and rheological properties of the water-solid bed interface in the Weser and Ems Estuaries, North Sea, Germany: Implications for fluid mud classification. *Journal of Coastal Research*, *29*, 797–808.

Richardson, J. F., & Zaki, W. N. (1954). The sedimentation of a suspension of uniform spheres under conditions of viscous flow. *Chemical Engineering Science*, *8*, 65–78.

Schoellhamer, D. H. (2011). Sudden clearing of estuarine waters upon crossing the threshold from transport to supply regulation of sediment transport as an erodible sediment pool is depleted: San Francisco Bay, 1999. *Estuaries and Coasts*, *34*(5), 885–899.

Talke, S. A., De Swart, H. E., & De Jonge, V. N. (2009). An idealized model and systematic process study of oxygen depletion in highly turbid estuaries. *Estuaries and Coasts*, *32*, 602–620.

Talke, S. A., De Swart, H. E., & Schuttelaars, H. M. (2009). Feedback between residual circulations and sediment distribution in highly turbid estuaries: An analytical model. *Continental Shelf Research*, *29*, 119–135.

Uncles, R. J., Joint, I., & Stephens, J. A. (1998). Transport and retention of suspended particulate matter and bacteria in the Humber-Ouse Estuary, United Kingdom, and their relationship to hypoxia and anoxia. *Estuaries*, *21*, 597–612.

Van Maren, D. S., Winterwerp, J. C., & Vroom, J. (2015). Fine sediment transport into the hyper-turbid lower Ems River: The role of channel deepening and sediment-induced drag reduction. *Ocean Dynamics*, *65*, 589–605.

Van Straaten, L. M. J. U., & Kuenen, P. H. (1957). Accumulation of fine grained sediments in the Dutch Wadden Sea. *Netherlands Journal of Geosciences*, *19*, 329–354.

Wang, X. H. (2002). Tide-induced sediment resuspension and the bottom boundary layer in an idealized estuary with a muddy bed. *Journal of Physical Oceanography*, *32*, 3113–3131.

Wang, L. (2010). Tide driven dynamics of subaqueous fluid mud layers in turbidity maximum zones of German estuaries (Ph.D. Thesis), University of Bremen.

Weilbeer, H. (2007). Numerical simulation and analyses of sediment transport processes in the Ems-Dollard estuary with a three-dimensional model. In T. Kusuda, H. Yamanishi, J. Spearman, & J. Z. Gailani (Eds.), *Sediment and ecohydraulics: Intercoh 2005*, *Proceedings in Marine Science* (Vol. 9, pp. 447–463). Elsevier. https://doi.org/10.1016/S1568-2692(08)80032-0

Winterwerp, J. C., Vroom, J., Wang, Z. B., Krebs, M., Hendriks, E. C. M., Van Maren, D. S., et al. (2017). SPM response to tide and river flow in the hyper-turbid Ems River. *Ocean Dynamics*, *67*, 559.

Winterwerp, J. C., & Wang, Z. B. (2013). Man-induced regime shifts in small estuaries—I: Theory. *Ocean Dynamics*, *63*, 1279–1292.

Winterwerp, J. C., Wang, Z. B., Van Brackel, A., Van Holland, G., & Kösters, F. (2013). Man-induced regime shifts in small estuaries—II: A comparison of rivers. *Ocean Dynamics*, *63*, 1293–1306.